Fiber Bragg grating regeneration at 450°C for improved high temperature sensing

Karima Chah,[1,*] **Kivilcim Yüksel,**[2] **Damien Kinet,**[1] **Nazila Safari Yazd,**[1] **Patrice Mégret,**[1] **and Christophe Caucheteur**[1]

[1]*Faculty of Engineering, Electromagnetism and Telecommunication Department, University of Mons, Boulevard Dolez 31, 7000 Mons, Belgium*
[2]*Electronics Engineering Department, Izmir Institute of Technology, TR-35430 Urla, Izmir, Turkey*
*Corresponding author: karima.chah@umons.ac.be

Type-I fiber Bragg gratings photo-inscribed in hydrogen-loaded B/Ge co-doped silica single-mode optical fibers have been regenerated efficiently at 450°C, which is the lowest temperature reported so far. The mechanical strength of the annealed fiber is preserved while ensuring temperature sensing of the regenerated gratings up to 900°C. Unlike low temperature cycles ($\leq$ 600°C), an annealing process at higher temperatures revealed faster regeneration for strong gratings. Changes in grating strength were also measured before the regeneration cycle. These behaviors suggest the contribution of different mechanisms to the regeneration process with different relative dynamics. © 2019 Optical Society of America

Fiber Bragg gratings (FBGs) have become a standard for sensing purposes [1]. They even outperform their electric counterparts in many application fields. In a harsh environment characterized by extreme physical and/or chemical conditions like in the automotive sector (combustion engine vehicles), electric power generation (gas turbines), or oil and nuclear industries, a precise control of high temperature (over 400°C) and/or strain is required [2,3]. Unfortunately, under these severe conditions, FBGs produced by standard UV inscription techniques suffer from practical limitations. Indeed, the reflectivity of Type-I FBG starts to decay when the temperature reaches 400°C [4]. To overcome this limitation, several techniques have been developed to increase the resistance of FBGs to high temperature. Grating types proposed so far are Type-IIa [5], Sn-doped silica gratings [6], chemical composition gratings (CCGs) [7], gratings produced by IR femtosecond laser pulses [3,8], and regenerated gratings (RFBGs) in a gas-loaded single-mode fiber and in loaded and unloaded photosensitive fibers [9–14]. This last technique consists in applying to an initial FBG (seed) a heating cycle that will erase it first and rebuild a new one on its "footsteps." Despite all these efforts, the sensing properties of FBGs at high temperatures as well as their long-term stability remain a controversial subject that requires further investigation. Glass-softening [9,12,13,14] is believed to be the key limitation for FBGs technology in this field of application. The very high temperature (700°C–1100°C) applied during the annealing process reduces the mechanical sustainability of the fiber. Ceramic and metal tubes applied before the annealing process have been demonstrated as a possible protection [15]. Most of the proposed solutions in the literature are oriented toward the improvement of temperature sensing capabilities accounting for regeneration efficiency (ratio between regenerated and seed grating reflectivities) and/or long-term thermal stability. Recently, a preannealing at 700°C was demonstrated to generate a high refractive index modulation of the regenerated grating in a standard single-mode fiber [16]. An isothermal annealing was also investigated to lower the regeneration temperature and increase the long-term stability of the gratings [17]. A regeneration temperature of 680°C and good efficiency were demonstrated in a hydrogen-loaded Ge/B co-doped fiber [18]. Only a few studies were dedicated to the strain-sensing performances of the RFBGs [2].

In this work, we investigate two annealing approaches. In the first one [18], the temperature is increased monotonously until reaching a plateau (700°C–1100°C). During this process the gratings go through a "fast" regeneration cycle where the so-called regeneration temperature (T_{Reg}), corresponding to the total erasure of the FBGs, is determined. In the second method, we set the plateau at a temperature well below T_{Reg} where FBGs undergo a "slower" regeneration cycle. The main goal is to lower as much as possible the temperature of the regeneration process within an acceptable time to preserve the mechanical robustness of the FBGs. Performance parameters like the regeneration efficiency, strain, and temperature sensitivities of the RFBGs and the high temperature operation limit were determined.

Prior to the inscription process of FBGs the photosensitive optical fiber (PS1250/1500) including 10 mol.% of GeO_2 and 14–18 mol.% of B_2O_3 is hydrogen-loaded under ~200 bar and 60°C for 30 h. Type-I FBGs (seed) were then produced with the phase mask technique and a 7 ns pulse duration ArF Excimer laser emitting at 193 nm with 5 mJ energy and a 50 Hz repetition rate. Different FBGs 10 mm long with a varying transmission minimum (T_{min}) at Bragg wavelength (λ_B) were produced (2.0–23.5 dB). For higher efficiency,

regeneration cycles were conducted without any preannealing as reported in [18]. FBGs were placed in a tubular furnace able to reach 1200°C with different heating rates. Both reflection and transmission spectra were monitored during and after the annealing process thanks to a FBG interrogator from *FiberSensing* of optimal acquisition (1 Hz). From the measured $T_{\min}$ we determined the reflectivity (R). The grating strength, which is proportional to the integrated coupling constant ICC [4], is derived:

$$ICC = \tanh^{-1}\sqrt{R} = \tanh\sqrt{1 - T_{\min}}. \qquad (1)$$

For comparison, the ICC normalized to its initial value ($\eta_{T_{\min}}$) is used. When only the reflection spectrum is recorded, the grating strength can be estimated from the full width at half-maximum [FWHM ($\Delta\lambda$)] of the grating normalized to its initial value ($\Delta\lambda_0$) [19]:

$$\eta_{\text{FWHM}} = \frac{\Delta n_m}{\Delta n_{m0}} \cong \frac{\Delta\lambda}{\Delta\lambda_0}, \qquad (2)$$

where Δn_m and Δn_{m0} denote, respectively, the refractive index modulation of the grating and its initial value. For each FBG, Δn_{m0} is calculated using coupled mode theory and reported in Table 1.

Typical transmission and reflection spectra before (seed FBG) and after regeneration (RFBG) are depicted in Fig. 1. The reflectivity is 65%, and 14% for the seed and regenerated FBG, respectively, yielding a regeneration efficiency ($\eta = R_{\text{RFBG}}/R_0$) of 21.5%.

In Fig. 2, we show the evolution versus time of temperature, normalized reflection power (η_{Rp} in blue), and grating strength calculated from Eq. (1) ($\eta_{T_{\min}}$ in red) and Eq. (2) (η_{FWHM} in black). The inset in Fig. 2 is a closeup of the graph between 100 and 120 min (gray band). This range depicts the regeneration process where the FBG disappears and starts to rebuild. The area with sparse filling shows that R power (η_{Rp}) can still be measured in contrast to $T_{\min}(\eta_{T_{\min}} = 0)$. Hence, to determine T_{Reg} it is better to use η_{Rp}. Before the FBG is erased, another important process occurs, the effect of which is well described

Table 1. R_0, Δn_{m0}, R_{Reg}, Regeneration Efficiency (η) and T_{Reg}

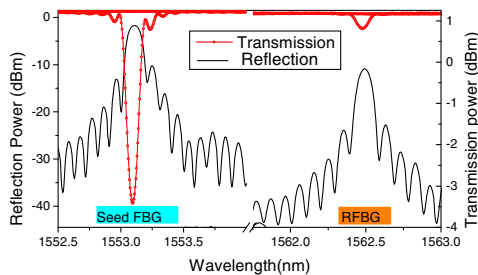| R_0 (%)	Δn_{m0}	R_{Reg} (%)	η (%)	T_{Reg} (°C)
37	$4.7 \cdot 10^{-5}$	11	29.7	709
50	$5.8 \cdot 10^{-5}$	17	34.0	688
65	$7.4 \cdot 10^{-5}$	14	21.5	623
98	$1.78 \cdot 10^{-4}$	36	36.2	617

Fig. 1. Reflection and transmission powers of seed and RFBG with initial reflectivity $R_0 = 65\%$.
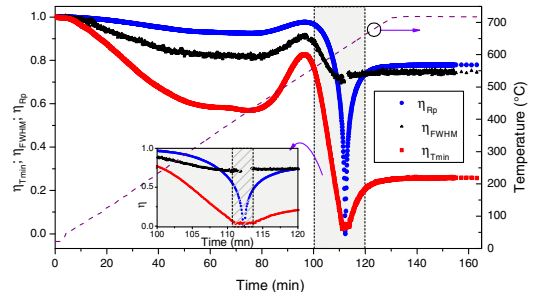

Fig. 2. $\eta_{T_{\min}}$, η_{Rp} and η_{FWHM} versus time during the annealing cycle for FBG with $R_0 = 65\%$.

by $\eta_{T_{\min}}$ since the reflection power saturates for strong FBGs and the FWHM cannot provide with high precision the changes in the FBG strength. Hence, an exponential decay of $\eta_{T_{\min}}$ is operated between 100°C and 230°C, and then the decay slows down until 400°C. The reflectivity of the FBG is reduced by more than 40%. Afterward, between 400°C and 550°C, the FBG recovers almost all of its initial strength before it starts to decay for the second time.

Similar low temperature changes (Fig. 2) have been reported in [20] and explained as a first regeneration regime, while in [21] FBGs instabilities are attributed to thermal annealing of the boron-related refractive index in the fiber. Chisholm *et al.* proposed a model based on both theories [22]: thermal decay of the UV-induced refractive index change of the grating [4] and thermal annealing of the boron-related refractive index of the fiber [23]. The negative average change in the refractive index is caused by the first mechanism starting at a low temperature, while the second one operates a positive change in the refractive index of the fiber core. This model did not account for the regeneration mechanism since the maximum used experimental annealing temperature was 475°C for 6 h. In a recent work on the regeneration of long period gratings inscribed in a boron-codoped germanosilicate single-mode fiber [24], a nonlinear temperature response of the grating with three threshold points has been observed. Owing to low transition temperature of germanium and boron, the observed effect has been correlated to the phase transition of glass (T_g) in the core and inner cladding at ~500°C and ~250°C, respectively, as well as the melting of inner cladding between 860°C and 900°C. In light of all these reported results, a possible explanation of our experimental finding—as its modeling is beyond the scope of this Letter—is that the first decrease in reflectivity is due to thermal decay of the UV-induced refractive index change [4–22]. The enhanced reflectivity around 500°C can be associated to an increase in the core effective refractive index [22] close to the T_g of the fiber core (annealing of boron), which becomes much larger than the negative average change in the refractive index due to decay of the UV-induced refractive index modulation. The observed second sharp decrease after 500°C can be linked to a release of internal stress due to both UV inscription (periodic stress) and to the high difference in doping concentration distribution between the fiber core and cladding [14]. This process has the advantage over the boron annealing effect and brings the reflection and transmission power under the limit of detection. This turning situation over the boron annealing effect implies that at least two mechanisms are behind the

UV-induced refractive index change: color center annealing (starting at low temperature) and stress-induced compaction [25]. Finally, the last increase in reflectivity, which corresponds to the rebuild of the FBGs, can be explained by thermal stabilization of internal and periodic stress relaxation and crystallization (α-quartz) that possibly occurred at low temperature because of stress induced-high pressure [14].

Therefore, in the first part of the experiments, we consider gratings of different reflectivities to determine their regeneration temperature (T_{Reg}) or more precisely their annealing temperature threshold for a fast regeneration process (~10 min) [18]. A high temperature and therefore fast annealing cycle are considered. The FBGs are heated with a ramp of 5°C/min up to 1100°C.

Figure 3 shows the R_{power} versus temperature for two FBGs with R_0 equal to 37% and 98%. One can see that the FBGs undergo a regeneration cycle from 620°C up to 800°C–900°C, and then they start to decay and erase completely at 1060°C (corresponding to the softening of the fiber core). Moreover, the FBG with the highest R_0 erases first and starts to regenerate as in [26]. This effect is outlined in Table 1, where T_{Reg} and the reflectivity of the regenerated grating (R_{Reg}) are summarized for seed FBGs of different R_0 and corresponding Δn_{m0}. As explained before, annealing of internal and UV-induced periodic stresses are responsible for the FBG erasure after compensation of the boron annealing effect. Highly reflective gratings because of higher UV exposure time show a higher stress effect. Therefore, at the activation energy of the process [25] the boron annealing effect is rapidly compensated in strong gratings, while it is still prevailing and screening the decrease in the weaker one.

In the second part of the experiments, we target lowering the annealing temperature to preserve the mechanical properties of the fiber and to compare the influence of the different proposed mechanisms involved in the fast regeneration cycle of FBGs. Two annealing temperatures below T_{Reg} are proposed: 600°C and 450°C. To reach the targeted temperatures, the FBG is heated rapidly with a rate of 12°C/min. Once the temperature is reached, the process requires less than 1 h for $T = 600$°C, while 150 h were needed for $T = 450$°C. These regeneration temperatures are the lowest used so far in a relatively short time since 450 h has been reported as a required time to decrease the regeneration temperature to 700°C for FBGs in standard SMF28 [16]. As explained previously, the fiber composition, mainly boron doping, which decreases the transition temperature of the core [24], and the 193 nm UV-induced defects type [13] contribute to lower the regeneration temperature. Figure 4 shows the annealing cycles at
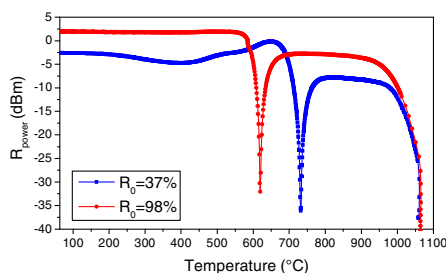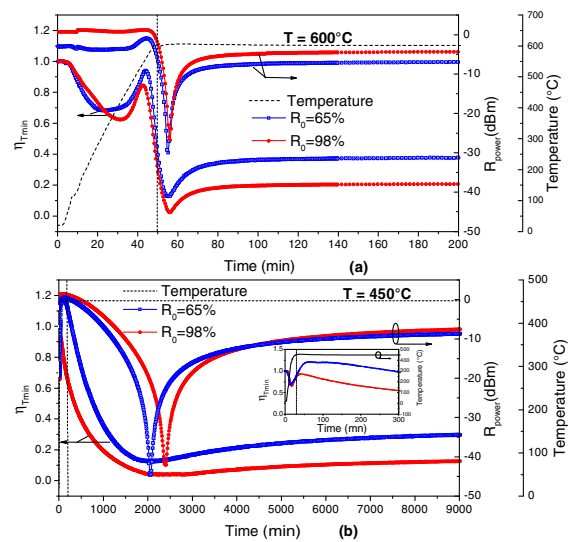

Fig. 4. Reflection power and $\eta_{T_{\min}}$ for FBGs with $R_0 = 65\%$ and $R_0 = 98\%$ during the annealing cycles at (a) 600°C and (b) 450°C.

600°C and 450°C for two FBGs with initial reflectivities 65% and 98%. The inset of the graph is a closeup showing the reflectivity changes, discussed previously, occurring when the temperature is still evolving linearly. Then the regeneration cycle occurs during the isothermal heating (at the targeted temperatures). It can also be observed, in contrast to the fast cycle, that FBG with $R_0 = 65\%$ erases before the one with $R_0 = 98\%$. The Bragg wavelength λ_B was also measured at room temperature before and after regeneration cycles. All the investigated gratings (65%–98%) show a wavelength red shift of (1.002–0.670) nm and (0.500–0.200) nm for regeneration at 450°C and 600°C, respectively. This red shift is linked to the boron annealing effect partially compensated by DC refractive index modulation decay. Both effects depend on Δn_{m0} and the annealing temperature, as reported in [22].

The total refractive index change involves different independent effects with different relative contributions [12,25]. These contributions decay at different absolute temperatures and at different times because of their own individual activation energy distribution [21,24,27]. Moreover, the same contribution at a given temperature $T1$ will take the required time to reach the activation energy to be involved in the process at another temperature $T2 < T1$ [4,25]. Therefore, as discussed before, the mechanism linked to the decrease in the FBGs reflectivities is mainly due to thermal decay of the UV-induced refractive index change, which includes both color center annealing and stress effects. The last process takes more time to contribute at a low temperature annealing cycle because of its high activation energy distribution (higher than that of color centers) [25]. Consequently, more time (slower process) is required for FBGs with a higher concentration of stress to regenerate when the temperature is lowered. Therefore, in the slow regeneration regime, FBGs with higher reflectivity regenerate later than the weaker ones.

Figure 5(a) depicts temperature calibration and a stability test of the grating at a high temperature. The regenerated FBGs show the same temperature behavior with the same sensitivities: (12.99 ± 0.18) pm/°C in the range 120°C–900°C

Fig. 3. Reflection power versus temperature for FBGs with $R_0 = 37\%$ and $R_0 = 98\%$.
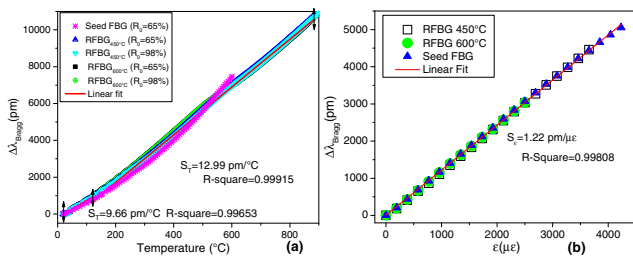
Fig. 5. (a) Temperature calibration curve of regenerated FBG at 450°C. (b) Strain calibration curve of seed and RFBG at 450°C.

and (9.66 pm/°C) in the range 20°C–120°C. They erase when the temperature exceeds 1000°C. We assume that this temperature corresponds to the glass softening one, since it is lower in a doped fiber (900°C–1000°C) than in pure silica glass [24]. For seed FBGs, the wavelength shift versus temperature is not linear. This effect is due to the negative contribution of the UV-induced refractive index change (thermal decay of the DC refractive index of the grating starting at a low temperature) and to the positive influence due to the thermal annealing of the boron-related refractive index of the fiber involved at a higher temperature ($\sim$400°C).

The low temperature regeneration process has the advantage of preserving the mechanical strength of the optical fiber [28]. Nevertheless, at 600°C and even lower at 450°C, the acrylate coating of the fiber cannot resist. One of the possible solutions is to use a reduced size oven to anneal the fiber at the location of the grating. Another potential solution is to use a metal coating as proposed in [15]. As a last step in our experimental work, a longitudinal strain calibration test was conducted on both the seed and regenerated gratings. Figure 5(b) reports the experimental results. The sensitivities in the investigated strain range are almost the same (1.22 ± 0.05) pm/$\mu\varepsilon$ for the seed and FBGs regenerated at 450°C and 600°C. Nevertheless, the breaking point for the FBGs regenerated at 600°C was found to be $\sim$2500 $\mu\varepsilon$ while the one for the FBGs regenerated at 450°C gratings is more than 3500 $\mu\varepsilon$.

In this work, we investigated the annealing temperature effect on FBGs produced in B/Ge codoped silica fiber of different strengths. Both a fast annealing cycle at a high temperature (>600°C) and slow annealing one at a lower temperature (450°C) have been experienced. A regeneration cycle at 450°C within 150 h has been demonstrated. Moreover, at this relatively low temperature, the weakest FBG regenerates faster than the higher ones while the opposite occurs for the high temperature cycle. These behaviors as well as changes in grating strength before the regeneration cycle suggest the competition between two main mechanisms in the annealing and regeneration process: boron-annealing induced refractive index changes of the fiber and a UV-induced refractive index change of the grating including color center annealing and stress-induced compactness of the fiber core.

The temperature sensitivity of RFBG was determined to be (12.99 ± 0.18) pm/°C in the range of 100°C–900°C, and longitudinal strain sensitivity is equal to (1.17 ± 0.01) pm/$\mu\varepsilon$.

REFERENCES

1. B. Lee, Opt. Fiber Technol. **9**, 57 (2003).
2. G. Laffont, R. Cotillard, N. Roussel, R. Desmarchelier, and S. Rougeault, Sensors **18**, 1791 (2018).
3. S. J. Mihailov, Sensors (Basel) **12**, 1898 (2012).
4. T. Erdogan, V. Mizrahi, P. J. Lemaire, and D. Monroe, J. Appl. Phys. **76**, 73 (1994).
5. Groothoff and J. Canning, Opt. Lett. **29**, 2360 (2004).
6. G. Brambilla and H. Rutt, Appl. Phys. Lett. **80**, 3259 (2002).
7. M. Fokine, J. Opt. Soc. Am. B **19**, 1759 (2002).
8. H. Chikh-Bled, K. Chah, Á. González-Vila, B. Lasri, and C. Caucheteur, Opt. Lett. **41**, 4048 (2016).
9. S. Bandyopadhyay, J. Canning, M. Stevenson, and K. Cook, Opt. Lett. **33**, 1917 (2008).
10. E. Lindner, C. Chojetzki, S. Brückner, M. Becker, M. Rothhardt, and H. Bartelt, Opt. Express **17**, 12523 (2009).
11. K. Cook, L. Y. Shao, and J. Canning, Opt. Mater. Express **2**, 1733 (2012).
12. J. Canning, M. Stevenson, S. Bandyopadhyay, and K. Cook, Sensors **8**, 6448 (2008).
13. J. Canning, S. Bandyopadhyay, M. Stevenson, P. Biswas, J. Fenton, and M. Aslund, J. Eur. Opt. Soc. **4**, 09052 (2009).
14. J. Canning, S. Bandyopadhyay, P. Biswas, M. Aslund, M. Stevenson, and K. Cook, in *Frontiers in Guided Wave Optics and Optoelectronics*, B. Pal, ed. (Intech, 2010), pp. 363–384.
15. D. Barrera, V. Finazzi, J. Villatoro, S. Sales, and V. Pruneri, IEEE Sens. J. **12**, 107 (2012).
16. P. Holmberg, F. Laurell, and M. Fokine, Opt. Express **23**, 27520 (2015).
17. M. Celikin, D. Barba, B. Bastola, A. Ruediger, and F. Rosei, Opt. Express **24**, 21897 (2016).
18. A. Bueno, D. Kinet, P. Mégret, and C. Caucheteur, Opt. Lett. **38**, 4178 (2013).
19. H. Patrick, S. L. Gilbert, A. Lidgard, and M. D. Gallagher, J. Appl. Phys. **78**, 2940 (1995).
20. L. Polz, Q. Nguyen, H. Bartelt, and J. Roths, Opt. Commun. **313**, 128 (2014).
21. S. Pal, Opt. Commun. **262**, 68 (2006).
22. K. E. Chisholm, K. Sugden, and I. Bennion, J. Phys. D **31**, 61 (1998).
23. I. Camlibel, D. A. Pinnow, and F. W. Dabby, Appl. Phys. Lett. **26**, 185 (1975).
24. W. Liu, K. Cook, and J. Canning, Sensors **15**, 20659 (2015).
25. G. Violakis and H. G. Limberger, Opt. Mater. Express **4**, 499 (2014).
26. S. Bandyopadhyay, J. Canning, P. Biswas, M. Stevenson, and K. Dasgupta, Opt. Express **19**, 1198 (2011).
27. S. Pal, J. Mandal, T. Sun, and K. T. V. Grattan, Appl. Opt. **42**, 2188 (2003).
28. T. Wang, L. Y. Shao, J. Canning, and K. Cook, Opt. Lett. **38**, 247 (2013).